Electronic Supplementary Information

Photo splitting of xylose and xylan to xylonic acid and carbon monoxide

Junqiang Zhang,[a] Kangning Liu,[a] Shaolong Sun,[b] Runcang Sun,[*a] Jiliang Ma[*a]

[a] Liaoning Key Lab of Lignocellulose Chemistry and BioMaterials, Liaoning Collaborative Innovation Center for Lignocellulosic Biorefinery, College of Light Industry and Chemical Engineering, Dalian Polytechnic University, Dalian 116034, China

[b] College of Natural Resources and Environment, South China Agricultural University, Guangzhou, 510642, China

*Corresponding authors' E-mail address: jlma@dlpu.edu.cn (Jiliang Ma) and rcsun3@dlpu.edu.cn (Runcang Sun), Tel.: +86-0411-86323652, Fax: +86-0411-86323652

1. Experimental section

1.1. Chemical reagents

Indium chloride (InCl$_3$, AR), thioacetamide (TAA, AR), and cadmium nitrate tetrahydrate (Cd(NO$_3$)$_2$·4H$_2$O, AR) were purchased from Shanghai Macklin Biochemical Co., Ltd (Shanghai, China). Sodium alginate (ALG, AR) was obtained from Sinopharm Chemical Reagent Co., Ltd (Shanghai, China). Potassium hydroxide (KOH, AR), xylose (AR), lactic acid (AR), xylan (AR), acetic acid (AR), formic acid (AR), glyceraldehyde (AR), tryptophan (Trp, AR), *p*-benzoquinone (BQ, AR), *p*-phthalic acid (PTA, AR), ethylenediaminetetraacetic acid (EDTA, AR) and other reagents were all purchased from Shanghai Aladdin Chemical Reagent Co., Ltd (Shanghai, China).

1.2 Characterization

The microstructure and morphology of all samples were explored by scanning electron microscopy (SEM, Hitachis-4800) and transmission electron microscopy (TEM, JEM-2100 CXII). N$_2$ adsorption-desorption isotherm measurements were performed on a physisorption analyzer (Micromeritics, ASAP 2020) at 77 K for *P/P$_0$* of 0.01-0.99. The specific surface area (N$_2$ adsorption-desorption, 77 K) isotherms were obtained by the Brunauer-Emmett-Teller method (BET) using a Micromeritics ASAP 2020 apparatus. Prior to adsorption experiment, all samples were degassed at 200 ^{o}C for 12 h under vacuum. The powder X-ray diffraction (XRD) patterns were collected in the *θ-2θ* mode using a Bruker D8 Focus diffractometer (CuKα radiation, λ = 0.15418 nm), operated at 40 kV and 40 mA with a scattering angle (2*θ*) of 5-80°. Fourier infrared (FT-IR) spectra of CdIn$_2$S$_4$ (CIS) and CIS/GO@3D-OMA were recorded on a Bruker Tensor 27 spectrophotometer in the range of 400-4000 cm^{-1} with a resolution of 4 cm^{-1}. A KBr disk containing 1% (w/w) finely ground sample was used for measurement. The X-ray photoelectron spectroscopy (XPS) analysis was performed with a Kratos Axis Ultra DLD spectrometer employing an amonochromated AlKR X-ray source (1486.6 eV). All samples were mounted using double-sided adhesive tape. The ultraviolet-visible diffuse reflectance spectra (UV-vis DRS) of CIS/GO@3D-OMA and CIS were detected by using a Cary 5000 spectrophotometer fitted with an integrating sphere attachment from 300 to 800 nm.

Ultraviolet photoelectron spectroscopy (UPS) was measured by using a He I (21.22 eV) as monochromatic discharge light source and a VG Scienta R4000 analyzer. A sample bias of -5 V was applied to observe the secondary electron cutoff (*SEC*). The work function can be determined by the difference between the photon energy (21.2 eV) and the binding energy of the secondary cutoff edge. The photoluminescence (PL) spectra were recorded by an Edinburgh FLS-920 spectrometer at room temperature. The Raman spectra were recorded from 500 to 2500 cm^{-1} on a Raman spectrometer (Thermo Fischer DXR). Electron spin-resonance spectroscopy was used to study molecules and materials with unpaired electrons, and the 5,5-dimethyl-1-pyrroline N-oxide (DMPO) was chosen as a spin trap for the detection of hydroxyl radical ($\cdot$OH) and superoxide ($\cdot O_2^-$), the 2,2,6,6-tetramethylpiperidine-1-oxyl (TEMPO) was applied to characterize electrons and holes, while the amino-2,2,6,6-tetramethylpiperidine (TEMPONE) was used to detect singlet oxygen.

1.3 Photoelectrochemical measurements

Electrochemical measurements were carried out on a CHI660E electrochemical workstation with a stand three-electrodes system. Among them, a Pt wire was used as the counter electrode, and the reference electrode was the saturated Ag/AgCl. The cleaned F-doped tin oxide (FTO) glass was used as the working electrode. 5 mg of corresponding photocatalyst and 20 μL of Nafion (5%) were added into 0.98 mL of ethanol to form a homogeneous slurry. The homogeneous slurry was ultrasonic for 30 min and then coated on the FTO glass. The obtained system was dried at 150 ^{o}C for 60 min. The supporting electrolyte was Na_2SO_4 solution (0.5 M) with the pH value of 6.8. The incident visible light source was Xe lamp (300 W).

The electrochemical impedance spectroscopy (EIS) was detected by an AC voltage amplitude of 10 mV at -0.3 V versus Ag/AgCl over the frequency range from 10 kHz to 0.01 Hz in the irradiation of Xe lamp. The Mott-Schottky was studied in the electrolyte of Na_2SO_4 (0.5 M), and the frequency of the AC potential was set as 500, 800, and 1000 Hz as well as the amplitude was 5 mV.

2. Results and discussion
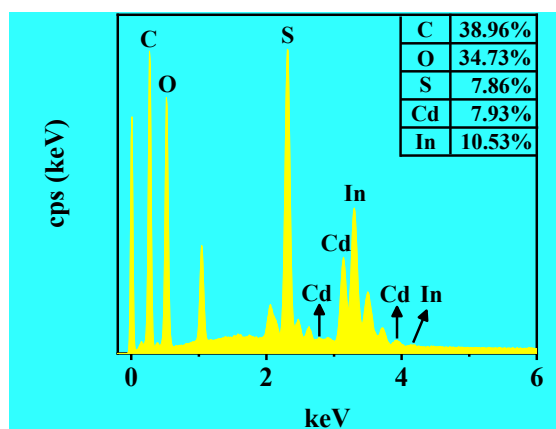
Fig. S1. The EDS spectrum of CIS/GO@3D-OMA-3.
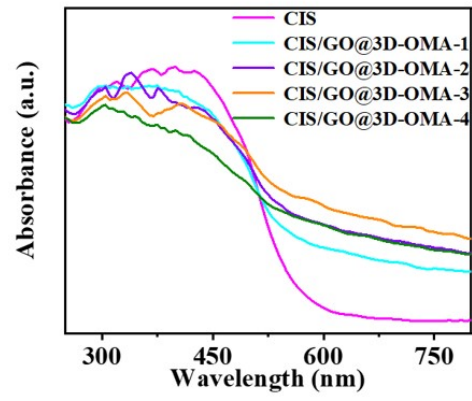
Fig. S2. Ultraviolet-visible diffuse reflectance spectra of CIS and CIS/GO@3D-OMA.
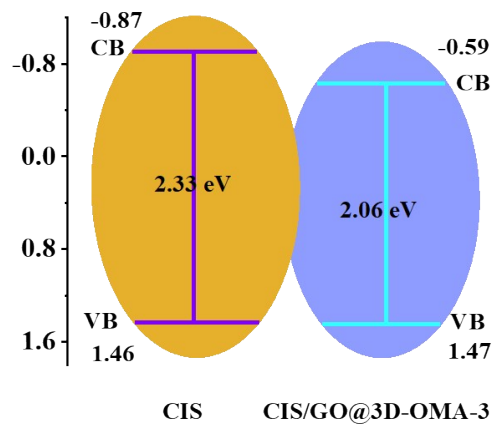
Fig. S3. The band energy diagrams of CIS and CIS/GO@3D-OMA-3.
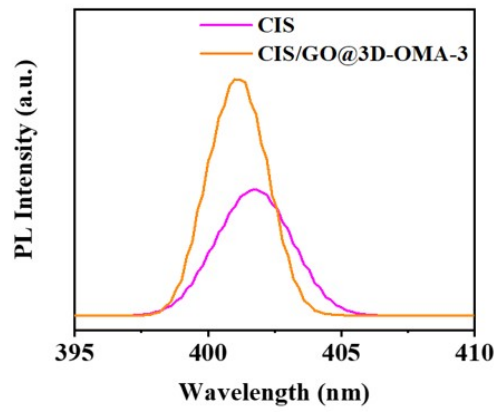
Fig. S4. The photoluminescence (PL) emission spectroscopy of CIS and CIS/GO@3D-OMA-3.
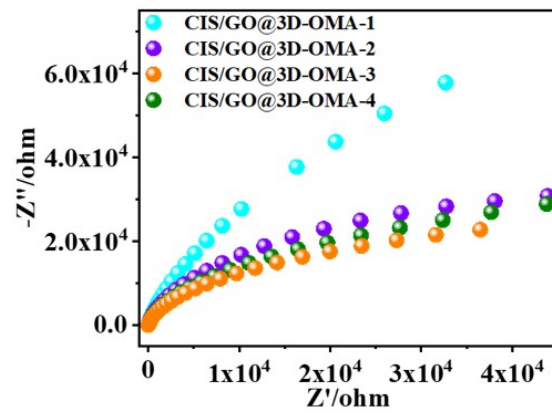
Fig. S5. The electrochemical impedance spectroscopy of CIS/GO@3D-OMA.
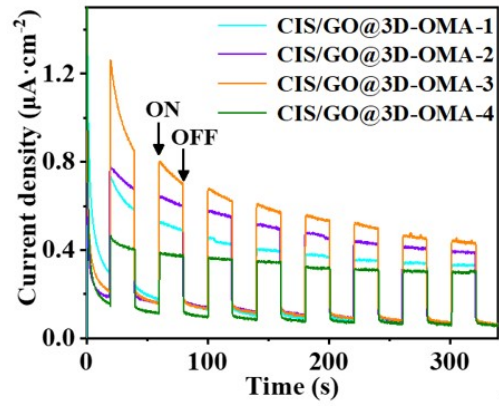
Fig. S6. The photocurrent response plots of CIS/GO@3D-OMA.
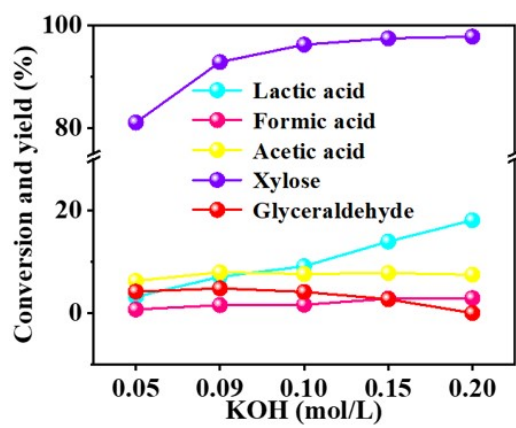
Fig. S7. The effects of KOH concentration on the conversion of xylose via CIS/GO@3D-OMA-3.
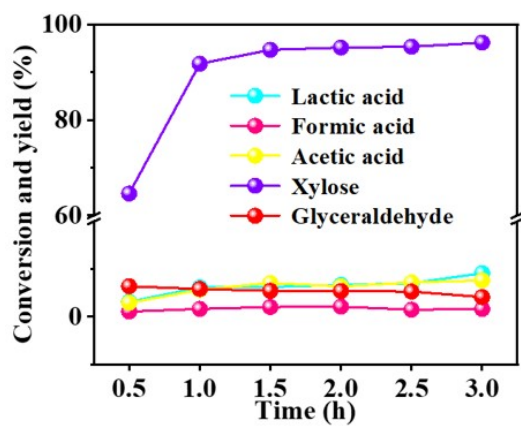
Fig. S8. The effects of reaction time on the conversion of xylose via CIS/GO@3D-OMA-3.
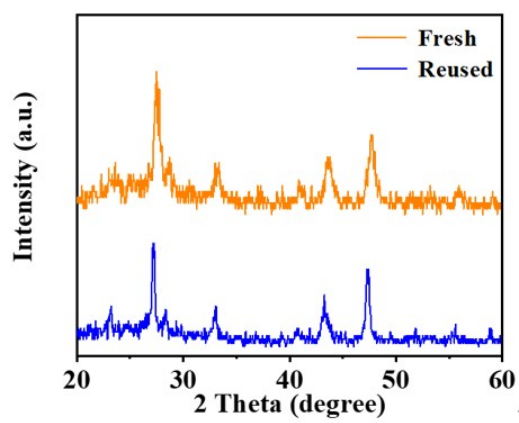
Fig. S9. XRD of fresh and reused CIS/GO@3D-OMA-3.
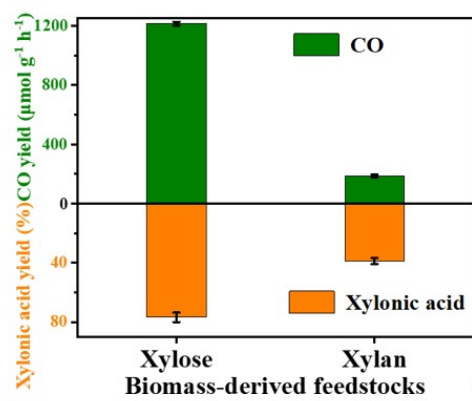
Fig. S10. Universality tests of CIS/GO@3D-OMA-3.
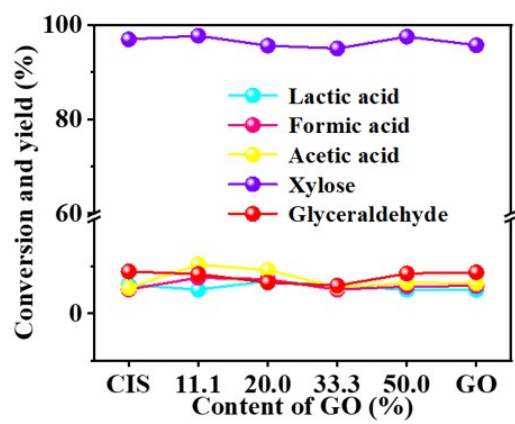
Fig. S11. The effects of GO, CIS, and the GO dosages in CIS/GO@3D-OMA on the conversion of xylose.